ELSEVIER

Materials Science and Engineering A 344 (2003) 1–9

MATERIALS SCIENCE & ENGINEERING A

www.elsevier.com/locate/msea

Microstructural changes due to laser ablation of oxidized surfaces on an AISI M2 tool steel

M.S.F. Lima [a,*], N.D. Vieira, Jr. [a], S.P. Morato [b], P. Vencovsky [c]

[a] *Center for Laser and Applications, IPEN-Trav. R 400, 05508-900 São Paulo, Brazil*
[b] *LaserTools Technologia Ltd., Trav. R 400, 05508-900 São Paulo, Brazil*
[c] *Brasimet Com. Ind. SA, Av. Nacoes Unidas 21476, 04795-912 São Paulo, Brazil*

Received 13 September 2001

Abstract

Surface modifications due to high intensity laser interaction on oxidized M2 steels were studied by optical and electron microscopy, and X-ray diffraction. First, it was shown that surface ablation of the oxide layer was possible when the laser fluency was above 0.4 J cm^{-2}. Above this threshold, the surface presented craters due to the spread of the liquid metal. Second, it was demonstrated that the region near to the surface was partly transformed. The prior carbides were dissolved in the liquid metal and the martensite was decomposed during heating. During the rapid cooling, part of the austenite was retained and the remelted zone showed lower hardness than the matrix. A chemical homogeneous layer at surface balanced this hardness decrease.

Keywords: Laser processing; Laser ablation; Microstructural characterization; Phase transformations in metals and alloys

1. Introduction

AISI M2 steels are high-speed tool materials consisting of carbides, martensite and some residual austenite, and present high hardness and good thermal stability [1]. These properties can only be obtained by a convenient heat treatment of the as-cast alloy. In general, this type of steel is maintained at some high temperature, e.g. 1200 °C, to stabilize and to homogenize the austenite. This austenite is transformed to martensite during quenching, thus giving a high toughness material. Further treatment at intermediate temperatures, e.g. 560 °C, relaxes some transformation stresses and transforms the retained austenite to ferrite [2]. Once realized at normal atmosphere, these steps usually lead to surface contamination and to massive oxidation that must be removed either mechanically, e.g. by using sandblast, or chemically.

Laser cleaning offers competitive advantages to sandblast and chemical treatments because of the easy automation, the effluent elimination and the possibility to treat three-dimensional pieces, like drills and saw tips. Laser cleaning involves the removal of undesirable layers using short-time high-energy light pulses. The process can be athermal for the substrate when the layer is an oxidized film which detaches due to the rapid expansion of the brittle oxide metal together with the explosion of entrapped gases near metal–oxide interface [3]. Another possibility is the vaporization of a submicrometric layer by ablation [4]. Ablation is the effect of a rapid transition from superheated liquid to a mixture of vapor and liquid droplets [5]. Part of the incident heat can effectively be absorbed into the bulk material leading to local temperature changes and to structural modifications. These modifications can be deleterious for the material properties, depending on the desired application. Some laser cleaning techniques have

* Corresponding author. Tel.: +55-11-3816-9307; fax: +55-11-3816-9315.
E-mail address: mlima@net.ipen.br (M.S.F. Lima).

0921-5093/02/$ - see front matter
PII: S0921-5093(02)00051-5

used more power than needed to clean the surface to produce some surface roughness throughout melting, since a slightly rough surface can present superior adherence to coatings [6]. On the other hand, hard-enable materials, like tool steels, can present mechanical weaknesses at the surface when re-heated. Changes in the microstructure, in particular the dissolution of carbides and the re-austenitization of the martensite, leads to a combination of a soft surface layer on a hard substrate. However, the process involves high cooling rates and then martensite can be partially or entirely recovered leading to some surface hardness.

Colaco and Vilar [7] investigated the effect of laser remelting on the surface microstructure of a 13%Cr tool steel. These authors demonstrated that rapid solidification greatly increases the austenite fraction in the remelted zone. During cooling, this supersaturated austenite was transformed to martensite plus a fine network of carbides conferring a hardness level comparable but inferior to the as-tempered matrix: 570 and 420 HV for the tempered and laser remelted samples, respectively.

Rapid solidification increases the solubility of elements in the austenite, producing more chemical homogeneity. Gemelli et al. [8] demonstrated that laser surface remelting of a D2 tool steel produced an improved oxidation resistance at elevated temperatures without significantly affecting the tribological properties. These authors linked the oxidation resistance to the dissolution of chromium carbides and the consequent increase of Cr in the metallic solution. This phenomenon, known as passivation, is explained by the formation of a very thin chromium oxide layer at the material surface which protects the bulk material from corrosion.

AISI M2 steels are the tools material of choice for several applications and correspond for about 40% of the USA market for tools in weight. In Brazil, this class of steel represents about 80% of total manufactured weight for tool materials, with 2000 tons produced in 1998 [9]. Despite its importance, there is a lack of information about the laser cleaning of this class of steels and the influence of laser re-heating on the microstructure. The present study aims to establish a processing window for the elimination of oxidized layers on M2 steel samples using pulsed YAG lasers, as well as to investigate the microstructure modifications due to laser interaction.

2. Experimental

A 15-mm diameter cylindrical M2 steel bar was cut in pieces of 5-mm height. These samples were annealed at 1200 °C for 10 min and then quenched in a vacuum chamber. After they were tempered at 560 °C under an atmosphere composed of N_2 and H_2, twice, 2 h each time. The layer thickness is a few nanometers, as measured by scanning electron microscopy (SEM) in a region where a part of the layer was detached. Under this oxide layer, the as-tempered microstructure consisted of carbides embedded in a matrix of martensite and ferrite. The final hardness of the samples was between 62 and 64 HRC (Rockwell C test scale).

This work employed two different laser workstations. The first one was a passive Q-switched (PQS) Nd:YAG laser giving about 78 mJ energy per pulse during 20 ns, for a fixed frequency of 1 Hz. The second one was an active Q-switched Nd:YAG (AQS) laser giving an energy per pulse in the range 0.1–8 mJ, a pulse length between 100 and 600 ns, and a pulse frequency in the range 1–50 kHz. These lasers provided different intensities at the sample surface: for the PQS one obtains 1×10^8 W cm^{-2} at focus (2-mm focal spot diameter) or 2×10^7 W cm^{-2} when unfocused. For the AQS at focus (0.8-mm diameter) the intensity was in the range 4×10^5–1×10^7 W cm^{-2}.

Test surfaces of 3×3 mm^2 were scanned using a high-precision mechanical step motor (PQS) or a galvanometric head in line with the beam (AQS). The scanning was realized in a sequence of parallel lines at a fixed velocity and with 0.5 mm lateral shift. For the AQS laser experiments, the process was repeated twice for each square with 45° tilt in order to make the energy distribution uniform. For PQS tests this was not feasible due to experimental limitations. All laser experiments were carried out in normal atmosphere.

Microstructural observations were carried out using optical and SEM. Optical microscopy employed standard polishing techniques and Nital 10% for chemical etching [1]. SEM analyses were carried out using secondary or back-scattered electron images. Secondary electrons image revealed the topography of the sample. Images from back-scattered electrons provided different contrasts for different phase densities. In the present case, regions with low-density phases (such as carbides in iron) appeared brighter than dense phases. The identification of phases was achieved using X-ray diffraction (XRD) from the Cu Kα radiation line. The austenite/martensite volume ratio was calculated from the integrated peak intensities of XRD spectra using the Miller [10] formalism.

Microhardness tests were carried out using a Vickers equipment with applied load of 500 g. The resulting hardnesses were averaged with four consecutive tests at each surface. A standard deviation of about 18% was obtained after a series of 20 measurements in the same as-tempered iron surface.

The temperature evolution was calculated by a formalism proposed by Prokhorov et al. [11]. Considering a rectangular pulse shape, the temperature variation in depth, z, and time, t, after the expiration of the laser pulse, t_p, can be calculated as:

$$T(z,\ t > t_P) = T_0 + \frac{2a\phi\alpha^{1/2}}{k}\left\{t^{1/2}\mathrm{ierfc}\left[\frac{z}{2(\alpha t)^{1/2}}\right] - (t-t_P)^{1/2}\mathrm{ierfc}\left[\frac{z}{2(\alpha(t-t_P))^{1/2}}\right]\right\} \quad (1)$$

where t_p is the pulse length, T_0 is the ambient temperature, "a" is the absorption coefficient, ϕ is the intensity, α is the thermal diffusivity, k is the thermal conductivity and ierfc is the inverse of complimentary error function [12].

The temperature raise during laser pulse is correspondingly calculated by eliminating the second term within brackets in Eq. (1). Derivation of Eq. (1) in time and in depth gives the corresponding cooling rate ($\dot{T}$) and thermal gradient (G). The speed of a given isotherm was thus obtained by the quotient $\dot{T}/G$.

The absorption coefficient in the present case was considered as 35%, similar to that evaluated for the laser remelting of cast irons with the same radiation [13]. The thermal diffusivity and conductivity were considered as 9.7×10^{-6} m^2 s^{-1} and 51 W m^{-1} K^{-1}, respectively, as proposed by Ref. [14] for an AISI 1020 steel.

Thermodynamics calculations, including the partition coefficients of the elements during solidification, were performed using ThermoCalc software [15] using a generic SGTE solutions database. The influence of growth rate on the partition coefficient was analyzed using the Continuous Growth Theory proposed by Aziz [16], and it is presented in Eq. (2):

$$k_v = \frac{k_e + \frac{V}{V_D}}{1 + \frac{V}{V_D}} \quad (2)$$

where k_v is the effective partition coefficient, k_e is the equilibrium value of the partition coefficient (as given by ThermoCalc), V is the growth velocity and V_d is the diffusion velocity given by the ratio of the average diffusivity of the solutes in the liquid to the average distance of atoms in the liquid near interface.

The V_D values for each element were obtained in Refs. [17,18].

3. Results

3.1. Processing window

Different laser conditions were tested to check the efficiency of the oxide removal, as presented in Table 1. As can be seen, a range of intensities from 0.4 to 130 MW cm^{-2} was covered.

The experiments using the PQS laser produced the highest intensities of the ensemble due to the elevated pulse energy and the short pulse duration. When focused on the surface (PQS-1) the power density was sufficient to remove the oxide layer and also generated some remelting, as can be seen in Fig. 1a. Using the laser without a focusing optics (PQS-2) decreased the power density, and produced an uncompleted cleaned surface, Fig. 1b. Here however, the surface did not present indications of localized fusion.

The AQS experiments presented very good results for cleaning in all conditions except for the three lower power density tests (Table 1). The experiments AQS-8 and AQS-9 presented some residual oxide, particularly at the borders, and the AQS-10 did not affect the oxide layer. Fig. 2 presents micrographs of different processing conditions.

3.2. Calculations

The solidus and liquidus temperatures were calculated for the initial alloy composition (0.9%C, 4.25%Cr, 5%Mo, 6.2%W and 1.9%V in weight) giving 1195.17 and 1371.11 °C, respectively. Austenite, which is the first phase to grow, becomes supersaturated within the solidus–liquidus interval (mushy zone) generating M_6C below 1230 °C and MC below 1200 °C. At the tempering temperature, 560 °C, the equilibrium phases are ferrite, M_6C, and MC.

Departures from the local equilibrium at the solid–liquid interface may occur during solidification. The influence of growth velocity on the partition coefficient of the solutes was calculated using Eq. (2) and is illustrated in Fig. 3. Horizontal dashed lines are the equilibrium partition coefficient for each element. Solute trapping is noticed in speeds as low as 1 cm s^{-1} and becomes an important mechanism above 10 m s^{-1}.

The effect of an isolated pulse on the surface temperature of the sample is presented in Fig. 4a. The figure, calculated for the condition AQS-5, shows a melting period of about 110 ns followed by a rapid cooling rate near the liquidus, $\dot{T} = 8 \times 10^9$ °C s^{-1}. The isotherms velocity can be obtained from Eq. (1) as

$$VT = \frac{\partial T}{\partial t}\frac{\partial z}{\partial T}.$$

Fig. 4b presents the liquidus isotherm velocity (VT) calculated for three pulse lengths and showing the current experimental values. The lower VT limit is characterized by an excessive energy transfer to the sample, decreasing $\dot{T}$. A maximum temperature below the liquidus due to an insufficient laser power characterizes the "no melting" region.

Table 1
Experimental parameters of laser processing

	t_p (ns)	E_p (mJ)	ϕ (W cm^{-2})	f (Hz)	V_b (mm s^{-1})
PQS-1	20	78.0	1.3×10^8	1	0.5
PQS-2	20	78.0	2.0×10^7	1	0.5
AQS-3	100	7.7	9.8×10^6	1000	40
AQS-4	100	6.2	7.9×10^6	1000	40
AQS-5	100	4.9	6.2×10^6	1000	40
AQS-6	100	3.2	4.0×10^6	1000	40
AQS-7	200	0.8	9.8×10^5	10 000	40
AQS-8	200	0.6	7.9×10^5	10 000	40
AQS-9	200	0.5	6.2×10^5	10 000	40
AQS-10	200	0.3	4.0×10^5	10 000	40

PQS means passive mode Q-switched laser and AQS means active mode Q-switched laser, t_p is the pulse length, E_p is the energy per pulse, ϕ is the intensity, f is the pulse frequency, and V_b is the linear scanning speed.

3.3. Phase transformations

All successful experiments produced some surface melting of the metal. The surface was formed by a series of small liquid bath spots due to the pulsed laser. These laser marks produced only some small roughness for low power flux experiments and blow craters for the higher intensities, as shown in Fig. 5.

The comparison between secondary electrons (SE) and back-scattered electrons (BS) images allows observation of both the topography and the chemical variations at the remelted surface. Fig. 6 presents the same specimen area split in two different contrasts for SE (bottom-right) and BS (upper-left), both under SEM. White stains in the BS images represents zones where the carbides were only partially dissolved in the liquid. At the upper-right corner, a BS micrograph of the steel is presented, showing the initial distribution and size of the precipitates at the same scale.

The melt depth was very thin in the experiments, as can be seen in the optical microscopy of a transversal section Fig. 6. Only PQS-1 and AQS-3 experiments produced sufficient melt depth to be measured as about 5 and 2 μm, respectively. The heat-affected zones in all observations were negligible.

Fig. 7 presents the XRD spectra of the M2 steel surfaces with the oxide layer, after being ground to the base material, and after the laser treatments. The diffraction peaks were assigned only once, although they were observed in the same angle for several spectra. The as-TT material consisted of martensite and M_6C carbides covered by an oxide layer (Ox) of Fe_2O_3 and Fe_3O_4. The oxide peaks disappear from the spectra above AQS-9, showing the efficiency of the cleaning process over the AQS-7 test. Some carbide peaks can also be found in the AQS-7 and AQS-9 experiments, because of uncompleted dissolution. The austenite (γ) and martensite (α) phases were assigned with the respective Miller indexes. Austenite peaks were divided in two contributions, as presented in the detail in Fig. 8.

The relative volume ratios between austenite and martensite, $V_{\gamma/\alpha}$, were evaluated using the XRD spectra and are presented in Fig. 9. The initial value of $V_{\gamma/\alpha}$ for an alloy in as-tempered condition is about 6%. This

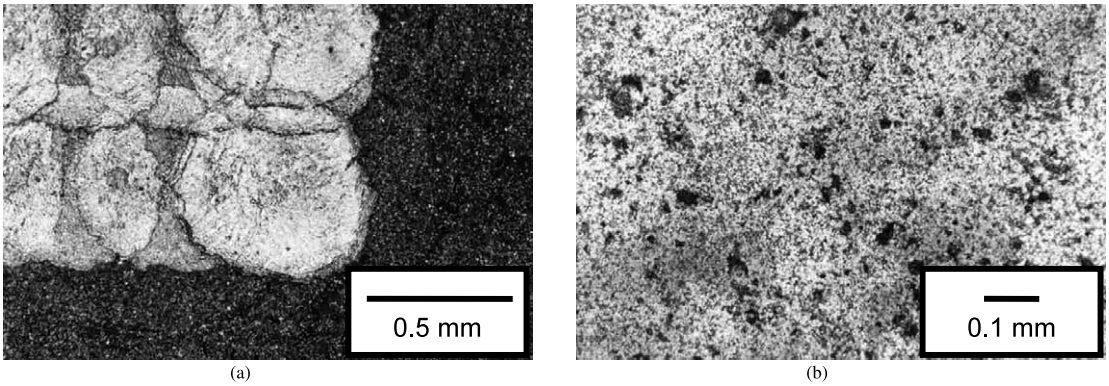

(a) (b)

Fig. 1. (a) PQS-1 laser processing marks near the border of the scanned window (optical microscopy with polarized light). (b) Uncompleted cleaned surface with the PQS-2 condition (optical micrograph).

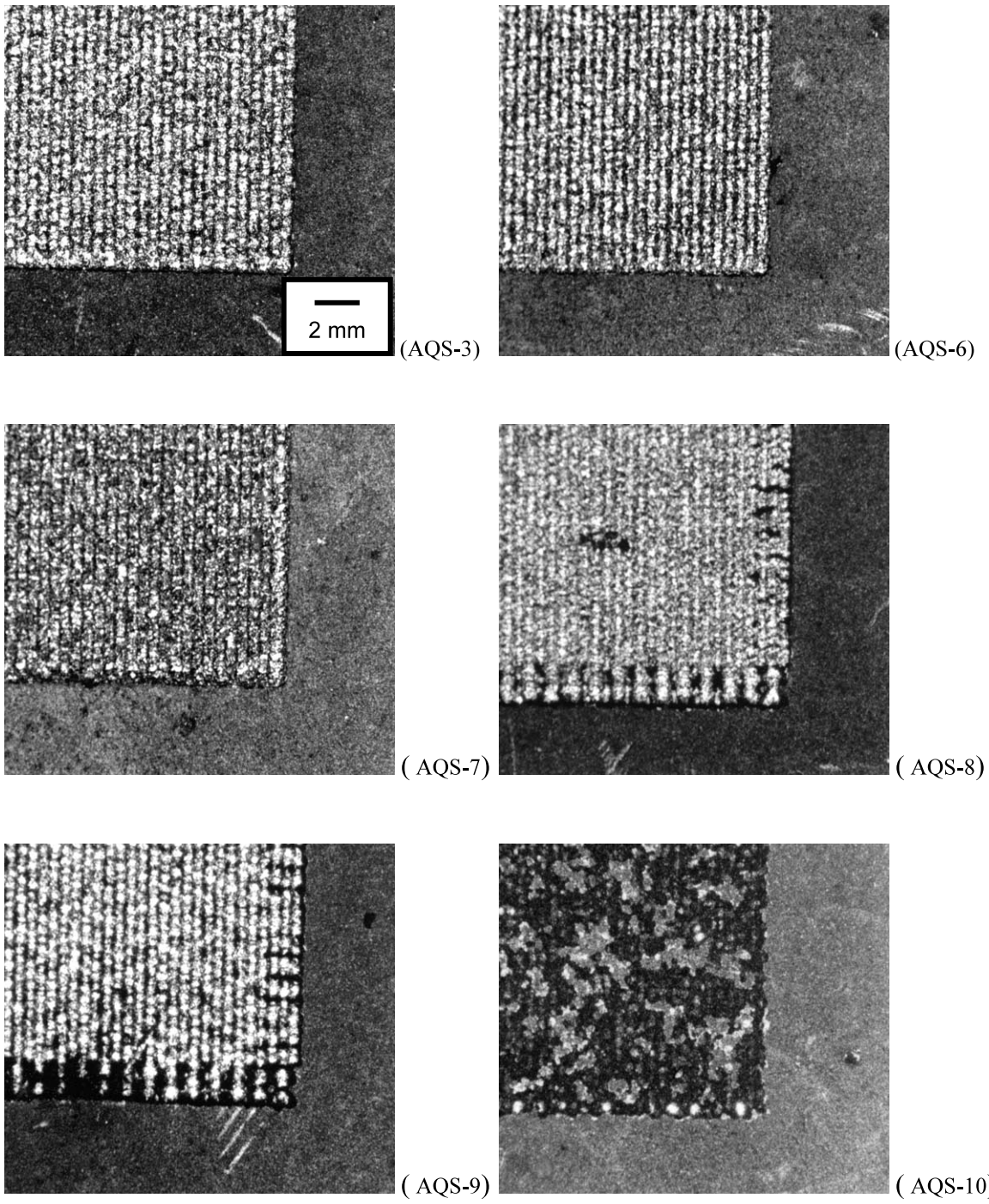

Fig. 2. Effect of the laser parameters on the macrostructure of oxidized samples. Only borders are presented. The scale applies for all photographs.

value is at the same order of the experiment AQS-9 where remelting was not verified. The value of $V_{\gamma/\alpha}$ was increased for power densities above 10^6 W cm^{-2}, reaching about 1/4 of retained austenite in volume.

The influence of the superficial austenite–martensite layer in hardness was then verified. The as-tempered grinded iron presented a hardness of 970 HV (67 Rockwell C). The hardness level for the laser treated surface under the conditions PQS-1 and PQS-2 was about 560 ± 20 HV. For the laser experiments using the AQS configuration where cleaning was achieved (AQS-3–7), the hardness was measured as 720 ± 60 HV.

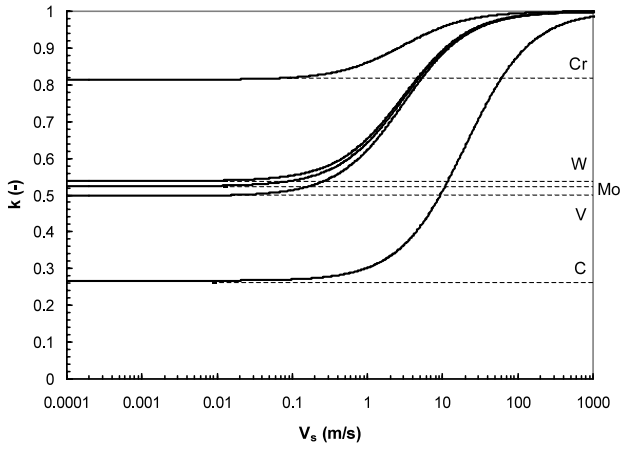

Fig. 3. The influence of the growth velocity on the partition coefficient of the elements.

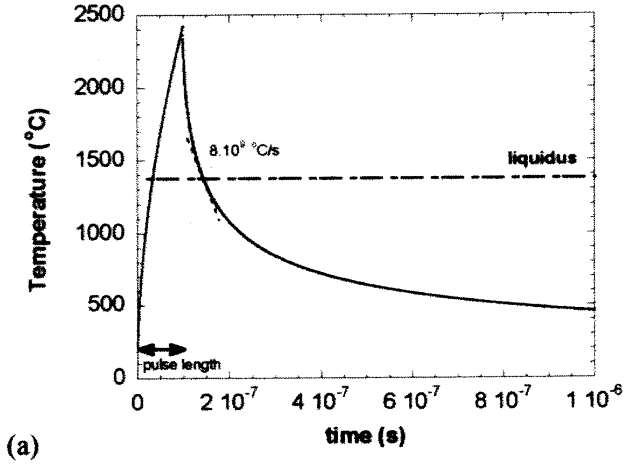

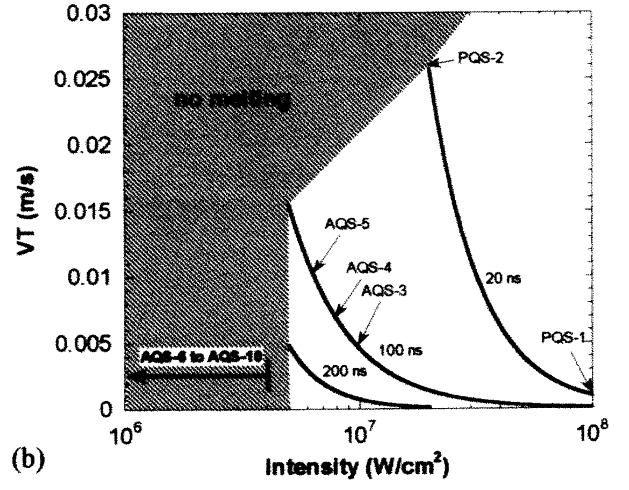

Fig. 4. (a) Thermal calculation of the surface temperature evolution in time for the AQS-5 condition. (b) Liquidus isotherm velocity as a function of laser parameters.

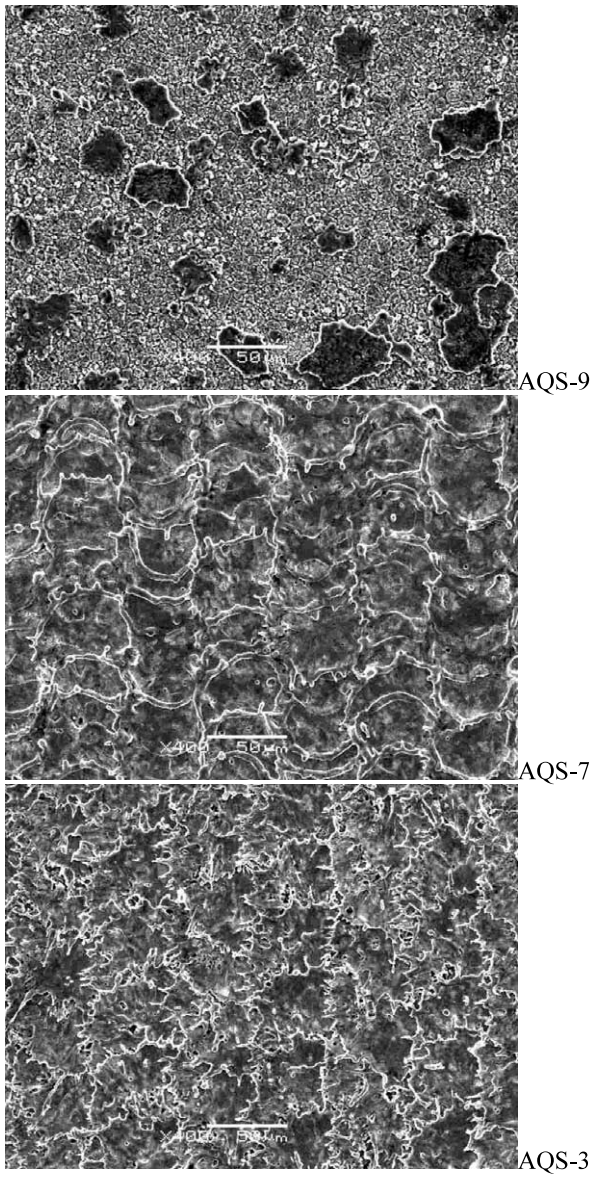

Fig. 5. Scanning electron micrographs showing different surface qualities for different process parameters. Secondary electrons images (SEM).

4. Discussion

The foremost advantage of laser processing is the speed. The experiments using the AQS configuration can clean a surface as larger as 100 cm^2 in less than 10 min. For the PQS processing, the beam scanned the sample at just 0.5 mm s^{-1} and the same surface might be cleaned in half a day. Experiments like the PQS-1 are interesting for applications if the laser can be pulsed at high frequencies and thus providing rapid processing speeds. On the other hand, the current active Q-switched (AQS) laser is one of the less expensive power lasers on the market and can be found easily in industry for another range of applications: marking, engraving and scribing. The possibility to clean metal surfaces, in

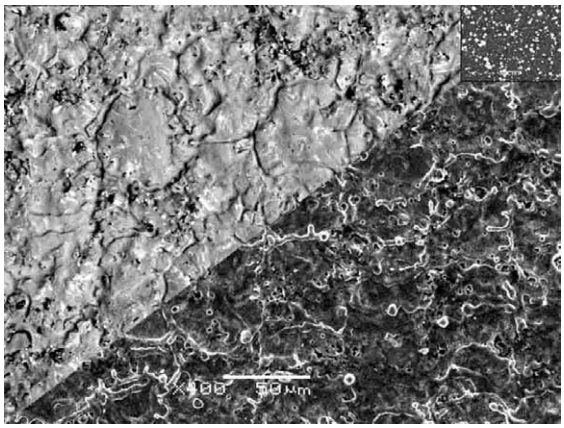

Fig. 6. Photomontage of three scanning electron micrographs. Bottom-right is a secondary electron image. Upper-left is a back-scattered electrons image. Upper-right is the back-scattered electrons image of base material. Scale applies for all photos. Condition AQS-5.

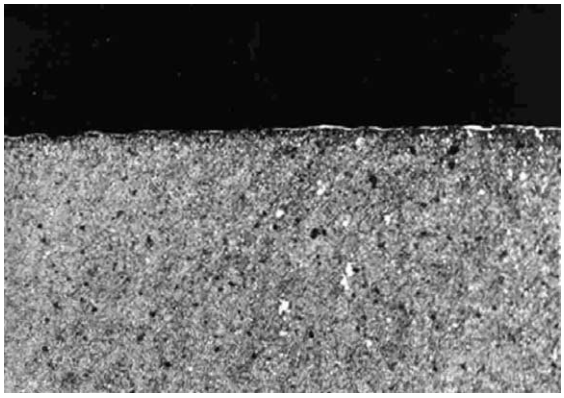

Fig. 7. Optical micrography of a transversal cut of the irradiated steel under AQS-3 condition. Laser processing was done in the upper surface. Optical microscopy. Etching: Nital 10%.

particular tools, using such ordinary lasers is then very attractive.

The mechanism of material removal is the laser ablation with vaporization of the base material. Using laser intensities on the range $1–2 \times 10^8$ W cm^{-2} for cleaning stainless steels after high temperature oxidation, Psyllaki et al. concluded that the mechanism was mechanical [2]. For these authors the oxide is detached due to the stresses normal to the oxide/metal interface. The difference between the present and Psyllaki's results comes from the different pulse lengths, which were 10 ns for this author. It could be conceived that such short interaction time can produce a mechanical shock wave [19]. This mechanical crackdown is possible for the PQS-2 condition at 2×10^7 W cm^{-2} and 20 ns. However, this was not a good cleaning condition, because some of the oxide still remained bonded to the surface. In the present case, the ablation mechanism is more efficient and allows a larger processing window, even if it produces some metal losses.

The best results for ablation were obtained when using low-frequency high power pulses. The high peak power ablates efficiently the surface at same time that the relative low frequency avoids the local increase in temperature thus inhibiting re-oxidation. Although the process was carried out in normal atmosphere, the processed surfaces were brightly metallic.

One megawatt per square centimeter seems to be the minimum intensity allowing surface ablation in AQS experiments. As can be seen in Fig. 2, below this limit the borders were not very well defined and some oxides remained on the treated surface. An exception occurs since the PQS-2 test was above the ablation intensity limit but the cleaning was incomplete. This is because of the low fluency in comparison with AQS-3 test. In fact, the AQS-3 experiment presented a fluency of 1 J cm^{-2}, which is more than the fluency of the PQS-1 and the PQS-2 tests: 0.6 and 0.1 J cm^{-2}, respectively. Considering now the laser fluency instead of the intensity, one can correctly assign the lower limit for the laser of the surfaces as 0.4 J cm^{-2}. It is also suggested to employ a second processing step were the laser scanning is shifted 90° to regularize borders.

Laser surface treatment changes the microstructure and influences the macroscopic properties. During heating, the martensite is re-austenitized and the fine dispersion carbides were dissolved in the matrix. As can be seen in Fig. 6, the carbides dissolution can be unequal in the matrix because the dissolution time is very short. The result was some small composition variations at the surface which led to a variation in the lattice spacing of the austenite, as observed in the XRD spectra (in the detail of Fig. 8).

Afterwards, since the cooling is very rapid (10^8–10^{10} °C s^{-1}), the martensite was formed again but some residual austenite was preserved. The carbides cannot be formed under these conditions, leading to a surface layer with reduced hardness. The hardness was lower for the PQS than for the AQS condition because the remelted layer was deeper for the PQS case. Thus in order to prevent low hardness at surface, AQS configuration must be used.

A high amount of austenite was detected at the PQS-2 surface although melting was not present. Some heat was transported to the volume during the irradiation because of the repetitive superposition, characterizing a solid-state transformation.

The liquidus isotherm velocity (VT) was in the order of a few centimeters per second, as can be seen in Fig. 4b. Although this is not the actual growth velocity of austenite (V), because this velocity changes in different regions, it is considered here as an average value of the solidification velocity in the entire liquid bath. This growth rate is not sufficient to produce solute trapping

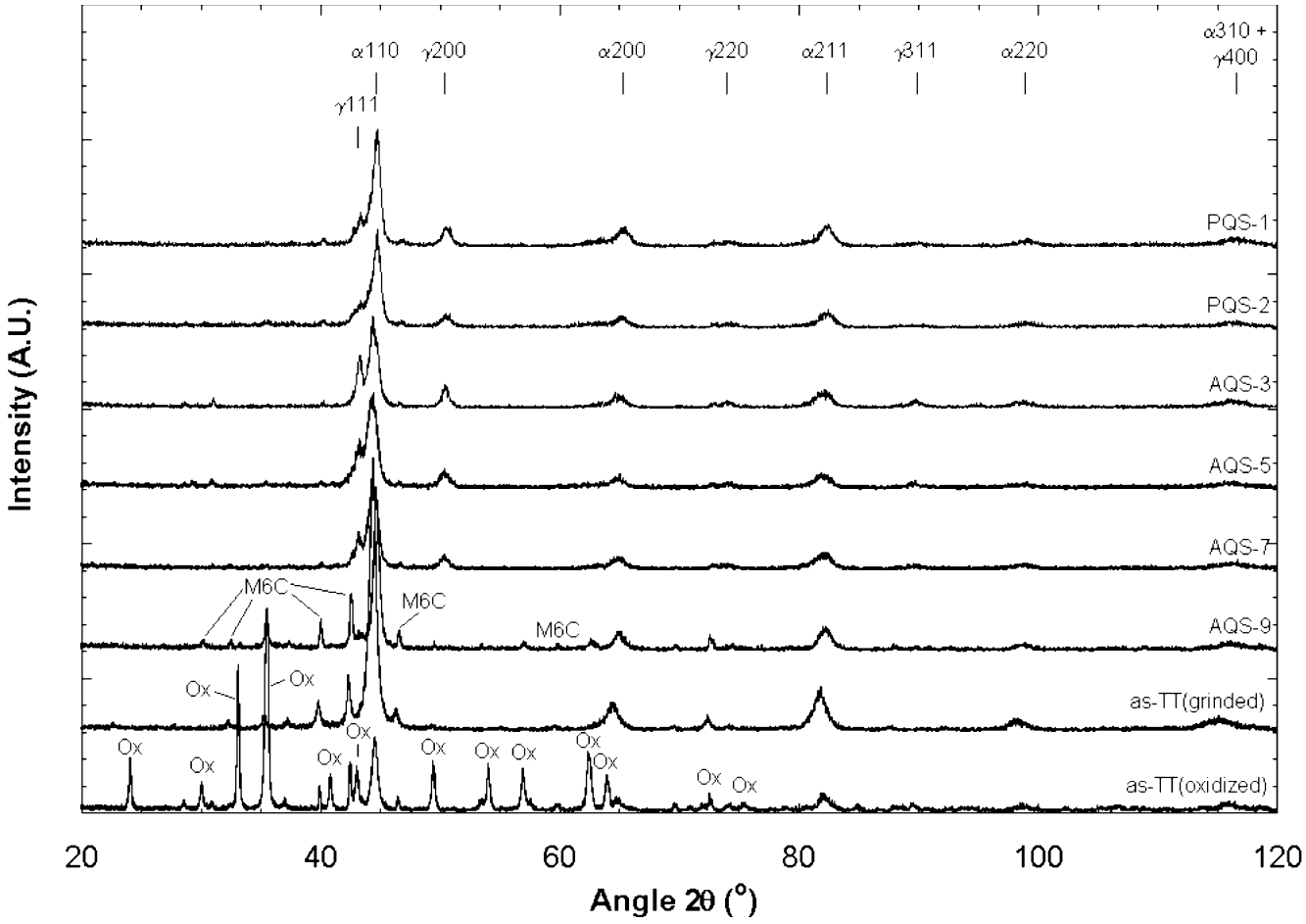

Fig. 8. XRD spectra of as-tempered and laser treated surfaces. See the text for legends. The detail in the AQS-3 spectrum shows a splitting of (220) peak of austenite.

effects (Fig. 3), meaning that the austenite had a composition very near the equilibrium value. However, this austenite has a high driving force for transformations, and it can be decomposed to ferrite plus carbides with a small increase in atomic mobility due to heating. It could be realized that the superficial metastable layer can be also transformed during the tool use. The metastable austenite is then transformed to martensite due to mechanical stresses.

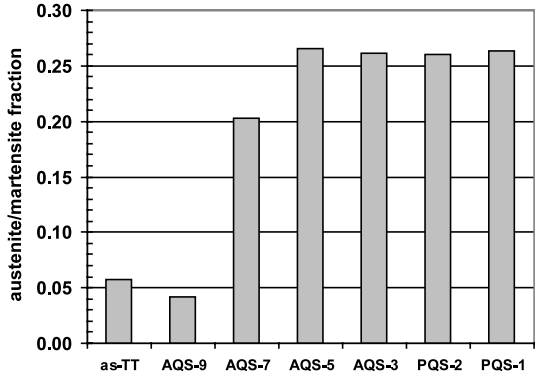

Fig. 9. The influence of process parameters on the austenite/martensite ratio at the surfaces, as measured from the XRD spectra.

The surface properties after laser ablation present some interesting brand new features. First, the surface composition is more homogenous and thus the protective oxide layer can be formed. If this austenite–martensite layer must be reduced to a minimum, one could choose to use the lower effective cleaning intensity of the processing window, i.e. AQS-7 condition. Second, an enhanced adhesion to a deposited layer can be obtained as the roughness is changed through process parameter. In particular, it must be observed that it generates a surface macrostructure near to the AQS-5 (Fig. 6) or the AQS-7 (Fig. 5) conditions instead of the AQS-3. This is because the blown craters in high-intensity tests forms metal tips (Fig. 5), which will eventually detach near to the metal-coating interface.

The deposition of a hard coating on the laser-cleaned surface is the next part of this work.

5. Conclusions

The main conclusions of this work can be summarized in the following way:

1. Complete surface cleaning of oxidized AISI M2 steel samples has been achieved using two different laser workstations. The best results were obtained when using the active Q-switched (AQS) laser in fluencies above 0.4 J cm^{-2} and at processing speeds of 40 mm s^{-1}.

2. The microstructure near the treated surface was changed. The martensite was decomposed in austenite and the carbides were dissolved in the matrix. However, due to short interaction time, the elements' distribution is unequal as observed in the scanning electron micrographs. The austenite peaks in the XRD spectra present doublets due to the different lattice parameters.

3. The irradiated surfaces lost part of their hardness due to the high content of austenite phase, about 25%. Nevertheless, the transformed layer is very thin and presents high driving force for transformation to martensite due to the metastability of the austenite structure. The fine roughness can also present better adherence to coating, as soon as the macrostructure can be controlled. The properties of a deposited coating on the laser-cleaned surface will be analyzed in a later work.

Acknowledgements

The authors would like to thank the Brazilian Synchrotron Light Laboratory (LNLS) for technical support. Thanks also are due to Professor Wilfried Kurz of the Department of Materials at the Swiss Federal Institute of Technology for the use of laboratory facilities. This work is funded by FAPESP—Fundação de Amparo à Pesquisa do Estado de São Paulo under grants 01/01195-2, 01/04159-7 and 01/04158-0. This work was realized under the CEPID network for an Optics and Photonics Research Center (http://watson.-fapesp.br/CEPID/centros.htm).

References

[1] American Society of Metals, Metals Handbook, vol. 9, 9th ed., ASM, Metals Park, OH, USA, 1985, p. 256.
[2] G.R. Speich, W.C. Leslie, Met. Trans. 3A (1972) 1043.
[3] P. Psyllaki, R. Oltra, Mat. Sci. Eng. A282 (2000) 145.
[4] A.M. Prokhorov, V.I. Konov, I. Ursu, I.N. Mihailescu, Laser Heating of Metals, Adam Hilger Series on Optics and Optoelectronics, 1990, USA, pp. 108–113.
[5] R. Kelly, A. Miotello, Appl. Surf. Sci. 96–98 (1996) 205.
[6] C. Coddet, G. Montavon, S. Ayrault-Costil, O. Freneaux, F. Rigolet, G. Barbezat, F. Folio, A. Diard, P. Wazen, J. Thermal Spray Tech. 8 (1999) 213.
[7] R. Colaco, R. Vilar, Scripta Mater. 38 (1) (1998) 107.
[8] E. Gemelli, A. Gallerie, M. Caillet, Scripta Mater. 39 (10) (1998) 1345.
[9] A.L. Costa e Silva, P.R. Mei, Aços e Ligas Especiais, 2nd edition, 1988, pp. 286–301 (in Portuguese).
[10] R.L. Miller, Trans. ASM 57 (1964) 892.
[11] A.M. Prokhorov, V.I. Konov, I. Ursu, I.N. Mihailescu, Laser Heating of Metals, Adam Hilger Series on Optics and Optoelectronics, 1990, USA, pp. 39–75.
[12] W. Gautschi, Error function and Fresnel integrals, in: M. Abramowitz, I.A. Stegun (Eds.), Handbook of Mathematical Functions, Dover Publications, New York, USA, 1972, pp. 295–330.
[13] E.M.R. Silva, W.A. Monteiro, W. Rossi, M.S.F. Lima, J. Mat. Sci. Lett. 19 (2000) 2095.
[14] H.A. Abel-aal, S.T. Smith, Wear 216 (1998) 41.
[15] ThermoCalc thermodynamic database (software), Version J, Stockholm Royal Institute, Sweden, 1994.
[16] M.J. Aziz, J. Appl. Phys. 53 (1982) 1158.
[17] T. Iida, R.I.L. Guthrie, The Physical Properties of Liquid Alloys, Clarendon Press, Oxford, UK, 1988, p. 232.
[18] W. Kurz, B. Giovanola, R. Trivedi, Acta Met. 34 (1986) 823.
[19] S.H. Jeong, R. Greif, R.E. Russo, Appl. Surf. Sci. 127–129 (1998) 1029.